Nonlocal Metasurfaces for Optical Signal Processing

Hoyeong Kwon[1,*], Dimitrios Sounas[1,*], Andrea Cordaro,[2,3] Albert Polman,[3] and Andrea Alù[1,4,5,6**]

[1]Department of Electrical and Computer Engineering, The University of Texas at Austin, Austin, TX, USA

[2]Institute of Physics, University of Amsterdam, Amsterdam, The Netherlands

[3]Center for Nanophotonics, AMOLF, Amsterdam, The Netherlands

[4]Photonics Initiative, Advanced Science Research Center, City University of New York, New York, NY 10031, USA

[5]Physics Program, Graduate Center, City University of New York, New York, NY 10016, USA

[6]Department of Electrical Engineering, City College of The City University of New York, NY 10031, USA

*These authors contributed equally to the paper

**aalu@gc.cuny.edu

Optical analog signal processing has been gaining significant attention as a way to overcome speed and energy limitations of digital techniques. Metasurfaces offer a promising avenue towards this goal, due to their efficient manipulation of optical signals over deeply subwavelength volumes. To date, metasurfaces have been proposed to transform signals in the *spatial* domain, e.g., for beam steering, focusing or holography, for which angular-dependent responses, or nonlocality, are unwanted features that must be avoided or mitigated. Here, we show that the metasurface nonlocality can be engineered to enable signal manipulation in the *momentum* domain over an ultrathin platform. We explore nonlocal metasurfaces performing basic mathematical operations, paving the way

towards fast and power efficient ultrathin devices for edge detection and optical image processing.

As large-scale image processing becomes important in many technological areas, the demand for integrated, faster and more efficient devices that can manipulate optical signals and images becomes more and more relevant. Currently, image processing is predominantly performed in the digital domain via integrated circuits, or in an analog fashion through bulky optical components [1]-[3]. The first approach offers great versatility in the operations that can be performed, but it suffers from microelectronic limitations regarding operational speed and power consumption, which grow rapidly with the size of the images to be processed. The second approach can overcome these limitations, however at the expense of a significantly larger size, which is unattractive in modern optical systems.

In another context, metasurfaces have been explored to efficiently manipulate the optical wavefront in the spatial domain over deeply subwavelength thicknesses [4]-[18], with the goal of imprinting a profile of choice to the impinging optical wave. Metasurfaces for beam steering, anomalous reflection and refraction, holography, light trapping and focusing have been recently developed, opening a successful route towards replacing bulky and complex optical components with ultrathin devices. In the following, we explore the use of metasurfaces to perform optical analog computing, manipulating the impinging optical wavefront in momentum space, rather than in the spatial domain.

Computing metasurfaces may combine the small size of digital systems with the high speed and near-zero power consumption of conventional optical components. A few proposals of engineered compact optical structures realizing Fourier optical processing have been recently put

forward [19]-[30]. A relevant example employed multilayered metamaterials [23], showing the possibility of performing linear mathematical operations over a footprint comparable to the wavelength, but at the cost of complex requirements on materials and fabrication. Another approach [26] was based on the excitation of surface plasmon polaritons at the interface between a dielectric prism and a plasmonic material. Interesting for its simplicity, this approach is however limited to differentiation in reflection mode, and it works for obliquely incident waves of narrow spatial spectrum and with limited efficiency, as it operates around the reflection zero associated with the plasmon resonance. Ref. [25] expanded this idea, proposing analog signal processing in transmission mode for normally incident signals based on suitably engineered photonic crystals, however, limited to the second derivative operation, and with similar limitations for efficiency and angular aperture, implying limitations on the overall achievable spatial resolution. All these approaches still require volumetric interaction with light, which limits the size of the metamaterial to the wavelength of operation.

In the following, we propose a new approach to impart linear mathematical operations on the impinging wavefront, based on nonlocal metasurfaces in transmission mode, providing large resolution and efficiency. By introducing a slow periodic spatial modulation over the metasurface profile, we significantly boost its nonlocal response, and through appropriate selection of the modulation parameters we can realize different types of mathematical operations. Here, to prove the principle, we use a basic sinusoidal modulation, adequate to realize basic operations, such as differentiation or integration. More sophisticated modulation profiles provide more degrees of freedom to engineer the nonlocal response, and therefore may allow the realization of complex mathematical operation with high accuracy. We demonstrate this concept for first- and second derivative and integration via a metasurface based on split-ring resonators,

but similar responses can be obtained with other metasurfaces, such as based on dielectric resonators, which may be suitable for optical frequencies. Our results pave the way towards the realization of efficient analog signal processing devices for edge detection and image processing operations [31],[32].

Consider a metasurface consisting of a periodic array of resonant particles in the *xy*-plane, as in Fig. 1a, here formed by split-ring resonators (SRRs) parallel to the *xz*-plane (magnetic dipole moment parallel to the *y*-axis) [33]. Other forms of resonant particles, such as dielectric resonators at optical frequencies, may yield similar results. Such a metasurface exhibits a transmission stopband at its resonance frequency f_0 for transverse magnetic (TM) waves propagating parallel to the *xz*-plane. As the incidence angle θ increases from 0 to 90 deg (θ is measured with respect to the *z*-axis), the resonance frequency remains the same, while the bandwidth scales by a factor proportional to $1/\cos\theta$ [34], as shown in Fig. 1b, which plots the transmission versus frequency and incidence angle. This nonlocal response results from the scaling of the transverse wave impedance of incident, reflected and transmitted waves versus the incident angle, and it is typically an undesired feature for metasurfaces and antenna arrays. This weak form of nonlocality, on its own, is not suitable for the purpose of analog signal processing, since a significant change in transmission is possible only around the grazing direction. Given that optical images impinging from the far-field have typically a spectral content focused over a narrow angular range within the normal direction, such a metasurface would require a complex lens system with a large magnification ratio, which may be bulky and challenging to design.

This problem can be overcome if we introduce a periodic modulation, such as a permittivity modulation in the SRR gaps $\varepsilon_n = \varepsilon_c\left[1+m\cos(2\pi na/p)\right]$, where ε_n is the

permittivity in the *n*-th SRR gap, ε_c is the average permittivity, m is the modulation amplitude, p is the modulation period and a is the distance between neighboring SRRs. Other forms of modulation, like changing the SRR size, which may be easier to achieve in practice, can lead to similar results [36]. Such a metasurface supports leaky-wave resonances, resulting from coupling of the incident waves to a surface mode along the metasurface [33]. The interference of these waves with the metasurface resonance results in a Fano response, as shown in Fig. 1c. For a given incident angle θ, the resonance frequency is determined by the frequency of the surface wave with wavenumber $k_0 \sin\theta + k_m$, where $k_m = 2\pi/p$ is the modulation wavenumber. This results in a strong variation of the resonance frequency with the incidence angle, following the dispersion of the surface mode. This property can be seen in Fig. 1d.

This strong nonlocal response can be used to realize different mathematical operations. For example, if the operation frequency is aligned with the transmission zero of the Fano resonance at normal incidence, due to the strong dispersion of the leaky mode associated with this resonance, the metasurface will exhibit a transmission coefficient that changes rapidly as we increase the incidence angle. This property can be seen in Fig. 2a, in which the transmission changes from zero at normal incidence to unity at an incidence angle of 39 deg. This metasurface can be readily used to implement the second derivative $-\alpha\, d^2/dx^2$ on the impinging wavefront, or $T(k_x) = -\alpha k_x^{\,2}$ in the spectral domain, where α is a constant. Fig. 2a compares the actual response of the metasurface with an ideal second-derivative response, showing very good agreement for incident angles smaller than 39 deg. This angle essentially provides the maximum spatial resolution of incident signals that can be processed by the metasurface, since finer details correspond to larger transverse wave numbers. Interestingly, by design we can tune the angle of

unitary transmission, and therefore the resolution of the metasurface and the high-*k* spectral features that we like to enhance, to any value of interest by simply engineering the geometrical parameters of the metasurface [36].

We stress that the response described above is the optimal response achievable with passive metasurfaces, for which transmission is restricted to values smaller than unity. Although ideally we would like α to be as large as possible, ensuring maximum edge enhancement, the fact that $|T(k_x)| \leq 1$ means that α is restricted to values smaller than $1/k_{x,max}^2$, where $k_{x,max}$ is the cutoff wavenumber of the input signal. By selecting $|T(k_{x,max})| = 1$, as in the metasurface of Fig. 2, we achieve the maximum possible α, and therefore the maximum possible efficiency for the second derivative operation. This should be contrasted with earlier approaches to analog computing, in which typically the transmission at the angle of maximum resolution is significantly smaller than unity, and this angle is also typically very small, drastically limiting the intensity of the output signal and the overall efficiency and resolution of image processing.

Figs. 2b-c show the effect of the metasurface described above on different 1D input signals, representing the incident magnetic field. The first one is a combination of rectangular functions, ramps, and a parabola in the transverse *x*-direction, as in Fig. 2b. The vertical discontinuities are assumed to occur within a finite distance, whose inverse approximately determines $k_{x,max}$. In our case, we chose this distance to be 0.78λ, where λ is the operation wavelength, in order for the spectral width to be approximately the same as the one of the metasurface. Upon transmission through the metasurface, linear segments are filtered out, parabolic segments are converted to flat ones, changes in the slope are transformed to delta-like functions and vertical jumps are transformed to pairs of delta-like functions pointing in opposite

directions (the flat segments resulting from the parabolic ones are hard to see, because they are obscured by the delta functions). This is exactly the response expected from a second derivative operation, which is also presented in Fig. 2b, for the same cutoff angle as the metasurface. Fig. 2c shows the effect of the metasurface on a sinusoidal signal. The output signal has the same form as the input (i.e., a sine/cosine function is transformed to a sine/cosine function), as expected from an ideal second derivative operation, also shown in the same figure.

Another important mathematical operation that in contrast to the second derivative has been less explored in the literature is the first derivative $\alpha\, d/dx$, which in the spectral domain has a transfer function $T(k_x) = i\alpha k_x$, where α is a constant. The fundamental reason why there has been less work on this arguably more basic operation is that it requires a transfer function with odd phase response with respect to the transverse wavenumber k_x. Obviously, such a response requires breaking the mirror symmetry with respect to the *x*-axis. Interestingly, however, mirror symmetry breaking is not enough, because of reciprocity. For example, consider a metasurface that is asymmetric with respect to the *x*-axis, but symmetric with respect to the *z*-axis, as in Fig. 3a. Reciprocity requires that transmission from direction 4 to 1, $T_{4\to1}$, is the same as transmission from direction 1 to 4, $T_{1\to4}$. If we now perform a mirror operation with respect to the *z*-axis, because of symmetry around *z* we find that $T_{2\to3} = T_{4\to1}$. Combining this condition with the one derived from reciprocity, we find $T_{2\to3} = T_{1\to4}$. $T_{1\to4}$ and $T_{2\to3}$ are the transmission coefficients for opposite k_x, showing that $T(-k_x) = T(k_x)$. It follows that, in order to implement an asymmetric $T(k_x)$ versus k_x, as required in the first-derivative operation, it is necessary to break both vertical and horizontal symmetry.

Based on the above remarks, we have modified the split-ring metasurface by adding a horizontally misplaced array of metallic wires parallel to the *x*-axis on one side of the SRR array, as in Fig. 3b, which allows breaking both horizontal and vertical symmetries at the same time. Controlling the unit cell geometry, we can achieve a response that approximates the first derivative operation, with a phase jump at $k_x = 0$, as shown in Fig. 3c. The deviations from the ideal response for larger k_x are due to the existence of higher order terms ($k_x^2, k_x^3, \ldots$) in the series expansion of $T(k_x)$ versus k_x, which cannot be cancelled with a simple periodic modulation and become more important as k_x increases. These terms can be rejected using more sophisticated modulation profiles, providing more degrees of freedom than a simple sinusoidal profile. Figs. 3d and 3e present the output through the metasurface for the same input signals as in the case of the second derivative. We can see that vertical jumps in the signal lead to delta-like functions, linear segments are converted to constant values, parabolic segments result in linear ones, and sine functions are converted to cosine ones, exactly as expected from a first derivative operation. The results are in very good agreement with the ideal first derivative response with the same cutoff angle, which is also presented in the same figure.

The metasurfaces presented so far can perform 1D operations. In order to extend these functionalities to 2D, we designed metasurfaces with a rotationally symmetric response. The simplest case consists in combining two identical 1D-operation metasurfaces rotated by 90 deg with respect to each other, as in Fig. 4a. Such a metasurface has a 90 deg rotational symmetry, and is expected to provide an identical second-derivative response for TM polarized waves along the *x*- and *y*-axes. This can be seen in Fig. 4b, which presents the transmission coefficient for TM waves versus θ (the elevation angle with respect to the *z*-axis) and φ (the azimuthal angle with

respect to the *x*-axis). Although the response is not azimuthally symmetric, as for an ideal Laplacian operator $\partial^2/\partial x^2 + \partial^2/\partial y^2$, which is the rigorous extension of the second derivative to 2D, as it will become clear in the following, this fact has in practice a negligible effect on the quality of the output images and the ability to perform edge detection.

Figs. 4c-f show the output from the metasurface and the ideal Laplacian operator with the same cutoff angle as the metasurface for an input 2D image with the initials of one of our institutions under illumination from the normal direction with *x*-polarized waves or unpolarized light. Details about how these results are derived are provided in [36]. For *x*-polarized illumination, the metasurface allows detection along the *x*-axis but not along the *y* one, due to the fact that according to design it performs edge detection only for TM waves, while the spectral components of the image associated with the edges along the *y*-axis have a pure TE polarization. The situation is reversed for *y*-polarized illumination (results for this case are provided in [36]). In this case, it is possible to detect edges along the *y*-axis but not along the *x*. This problem does not exist with an ideal Laplacian operator, which operates the same way on both TE and TM polarizations. However, if we use unpolarized light for the illumination of the image, as is the case in many realistic scenarios, we can detect well all edges, since in this case the incident light contains both orthogonal polarizations, which, as explained above, allow edge detection along orthogonal directions. This result is important from a practical perspective, as it shows that a perfectly azimuthally symmetric response, which is possible only over a region close to the normal direction, where the transmission and consequently the efficiency are small [25], may not be necessarily required in practice.

To conclude, we have shown how spatially modulated metasurfaces with appropriately engineered nonlocal response can be used to perform different types of mathematical operations on optical signals. We have demonstrated this for the 1D case of first and second derivative operations and in 2D for second derivative operations. Similar metasurfaces can also be used to achieve other linear operations, such as integration and image blurring, as discussed in [36]. In the examples provided in this paper, we have used a simple sinusoidal modulation, which imposes limitations on the complexity of the mathematical operations that can be performed. More sophisticated modulation profiles offer more degrees of freedom, which we are exploring at present. Our results have applications in analog image processing, particularly edge detection, as well as in the recently introduced concept of analog optical computation networks [23],[37]-[38].

This work was supported by the Air Force Office of Scientific Research with MURI grant No. FA9550-17-1-0002 and the Netherlands Organisation for Scientific Research (NWO).

References

[1] J. Nakamura, *Image Sensors and Signal Processing for Digital Still Cameras*, CRC Press, Boca Raton, FL, 2006.

[2] J. W. Goodman, *Introduction to Fourier Optics*, Robert & Company Publishers, Englewood, Co, 2005.

[3] H. Stark, *Application of Optical Fourier Transform*, Academic Press. Inc., New York, NY, 1982.

[4] N. Yu and F. Capasso, Flat optics with designer metasurfaces. *Nat. Mater.* **13**, 139–150, 2014.

[5] Y. Zhao, X.-X. Liu, and A. Alù, Recent advances on optical metasurfaces. *J. Opt.* **16**, 123001, 2014.

[6] S. A. Tretyakov, Metasurfaces for general transformations of electromagnetic fields. *Philos. Trans. R. Soc. London A* **373**, 20140362, 2015.

[7] S. B. Glybovski, S. A. Tretyakov, P. A. Belov, Y. S. Kivshar, C. R. Simovski, Metasurfaces: From microwaves to visible. *Phys. Rep.* **634**, 1–72, 2016.

[8] N. Yu, P. Genevet, M. A. Kats, F. Aieta, J.-P. Tetienne, F. Capasso, Z. Gaburro, Light propagation with phase discontinuities: Generalized laws of reflection and refraction. *Science* **334**, 333–337, 2011.

[9] A. V. Kildishev, A. Boltasseva, V. M. Shalaev, Planar photonics with metasurfaces. *Science* **339**, 1232009, 2013.

[10] S. Sun, K.-Y. Yang, C.-M. Wang, T.-K. Juan, W. T. Chen, C. Y. Liao, Q. He, S. Xiao, W.-T. Kung, G.-Y. Guo, L. Zhou, D. P. Tsai, High-efficiency broadband anomalous reflection by gradient meta-surfaces. *Nano Lett.* **12**, 6223–6229, 2012.

[11] F. Monticone, N. M. Estakhri, and A. Alù, Full control of nanoscale optical transmission with a composite metascreen. *Phys. Rev. Lett.* **110**, 203903, 2013.

[12] M. Esfandyarpour, E. C. Garnett, Y. Cui, M. D. McGehee, and M. L. Brongersma, Metamaterial mirrors in optoelectronic devices. *Nat. Nanotechnol.* **9**, 542–547, 2014.

[13] M. Kim, A. M. H. Wong, and G. V. Eleftheriades, Optical Huygens metasurfaces with independent control of the magnitude and phase of the local reflection coefficients. *Phys. Rev. X* **4**, 041042, 2014.

[14] Z. Bomzon, G. Biener, V. Kleiner, and E. Hasman, Space-variant Pancharatnam–Berry phase optical elements with computer-generated subwavelength gratings. *Opt. Lett.* **27**,

1141–1143, 2002.

[15] N. Mohammadi Estakhri and A. Alù, Wavefront transformation with gradient metasurfaces. *Phys. Rev. X* **6**, 041008, 2016.

[16] A. Epstein and G. V. Eleftheriades, Huygens' metasurfaces via the equivalence principle: Design and applications. *J. Opt. Soc. Am. B* **33**, A31–A50, 2016.

[17] V. S. Asadchy, A. Díaz-Rubio, S. N. Tcvetkova, D.-H. Kwon, A. Elsakka, M. Albooyeh, S. A. Tretyakov, Flat engineered multichannel reflectors. *Phys. Rev. X* **7**, 031046, 2017.

[18] Y. Ra'di, D. L. Sounas, and A. Alù, Metagratings: Beyond the limits of graded metasurfaces for wave front control. *Phys. Rev. Lett.* **119**, 067404, 2017.

[19] R. Slavík, Y. Park, M. Kulishov, R. Morandotti, and J. Azaña, Ultrafast all-optical differentiators. *Opt. Express*, **14**, 10699–10707 (2006).

[20] M. Ferrera et al. On-chip CMOS-compatible all-optical integrator. *Nat. Commun*, **29** (2010)

[21] J. Xu, X. Zhang, J. Dong, D. Liu, and D. Huang, High-speed all-optical differentiator based on a semiconductor optical amplifier and an optical filter. *Opt. Lett*, **32**, 1872–1874 (2007).

[22] A. Chizari, S. AbdollahRamezani, M. V. Jamali, and J. A. Salehi, Analog optical computing based on dielectric meta-reflect-array. *Opt. Lett*. 41, 3451–3454 (2016).

[23] A. Silva, F. Monticone, G. Castaldi, V. Galdi, A. Alù, and N. Engheta, Performing Mathematical Operations with Metamaterials, *Science*. **343**, 160-163 (2014).

[24] H. Chen, D. An, Z. Li, and X. Zhao, Performing differential operation with a silver dendritic metasurface at visible wavelengths, *Opt. Express.* **25**, 26417-26426 (2017).

[25] C. Guo, M. Xiao, M. Minkov, Y. Shi, and S. Fan, A Photonic Crystal Slab Laplace operator for image differentiation, *Optica*. **5**, 251-256 (2018).

[26] T. Zhu, Y. Zhou, Y. Lou, H. Ye, M. Qiu, Z. Ruan, and S. Fan, Plasmonic computing of spatial differentiation, *Nat. Commun.* **8**, 15391 (2017).

[27] S. Abdollahramezani, K. Arik, A. Khavasi, and Z. Kavehvash, Analog computing using graphene-based metalines, *Opt. Lett.* **40**, 5239 (2015).

[28] A. Pors, M. G. Nielsen, and S. I. Bozhevolnyi, Analog Computing Using Reflective Plasmonic Metasurfaces, *Nano Lett.* **15**, 791–797 (2015).

[29] A. Chizari, S. Abdollahramezani, M. V. Jamali, and J. A. Salehi, Analog optical computing based on a dielectric meta-reflect array, *Opt. Lett.* **41**, 3451 (2016).

[30] A. Youssefi, F. Zangeneh-Nejad, S. Abdollahramezani, and A. Khavasi, Analog computing by Brewster effect, *Opt. Lett.* **41**, 3467-3470 (2016).

[31] J. Canny, A computational approach to edge detection, *IEEE Trans Pattern Anal Mach Intel*. **8**, 679–698 (1986).

[32] D. Marr and E. Hildreth, Theory of edge detection. *Proc. R. Soc. Lond*. B 207, 187–217 (1980).

[33] Y. Hadad, D. L. Sounas, and A. Alu, Space-time gradient metasurfaces, Phys. Rev. B, vol. 92, p. 100304 (2015).

[34] This fact follows from Eq. 8 in [35] with $\chi_{ES}^{xx} = \chi_{ES}^{zz} = 0$.

[35] C. L. Holloway, E. F. Kuester, J. A. Gordon, J. O'Hara, J. Booth, and D. R. Smith, An overview of the theory and applications of metasurfaces: The two-dimensional equivalents of metamaterials, *IEEE Antennas Propag. Mag.* **54**, 10-35 (2012).

[36] Supplementary Information.

[37] Daniel R. Solli and Bahram Jalali, Analog optical computing, *Nat. Photonics*, 9. 704-706 (2015).

[38] A. M. Urbas et al. Roadmap on optical metamaterials, *J. Opt.* **18**, 093005 (2016).

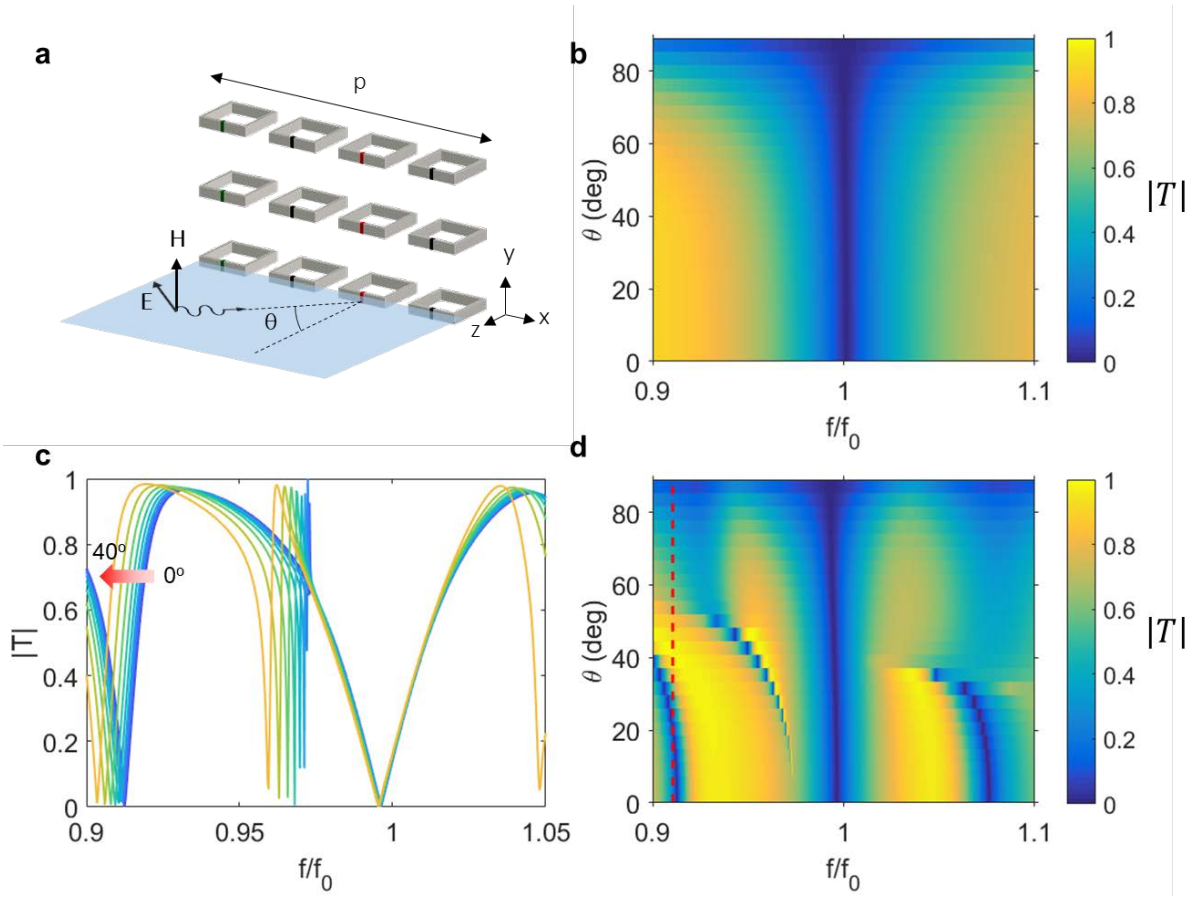

Fig. 1. Nonlocal metasurface. (a) Schematic showing an array of split-ring resonators parallel to the *xz*-plane. The metasurface is excited by TM polarized waves propagating on the *xz*-plane. (b) Transmission versus frequency and incident angle when all the SRRs in the metasurface are identical. (c) Transmission versus frequency for different incident angles when the SRRs are sinusoidally modulated in space parallel to the *x*-axis. The modulation is applied to the permittivity of the dielectric material in the SRR gaps. (d) Transmission versus frequency and incident angle for the same metasurface as in panel (c). The geometrical parameters are provided in [36].

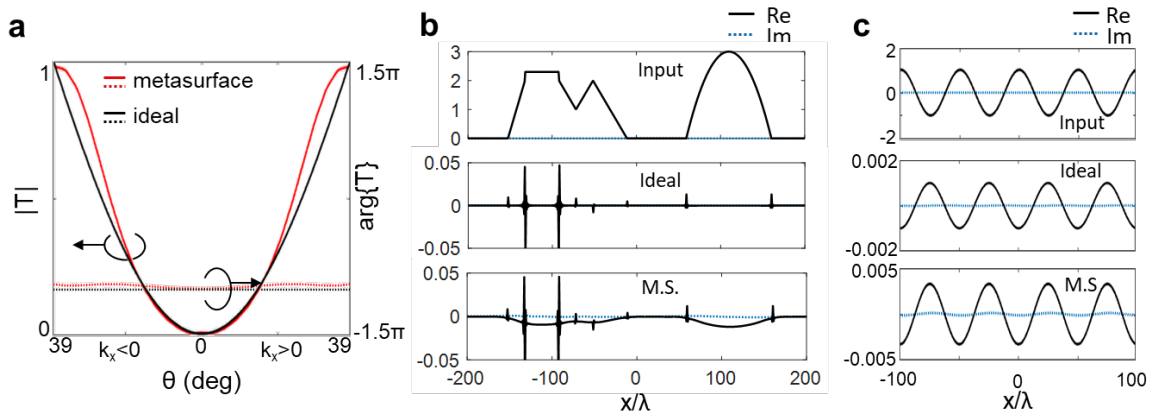

Fig. 2. Second derivative operation. (a) Transmission versus incident angle for the metasurface in Fig. 1c-d, for $f = 0.91 f_0$ (red dashed line in Fig. 1d). We also present the response for an ideal second derivative operation. The reference plane for the metasurface transmission is selected at a distance that leads to a 180 deg transmission phase at normal incidence. (b) Output of an ideal second derivative operation and of the metasurface when the top panel signal is applied as input. For the ideal response, we consider a cutoff angle of 39 deg (angle of unitary transmission for the metasurface). Here, we have discretized the input signal with a pixel size of 0.79λ, assumed to be the distance over which the vertical jumps occur. (c) Same as in panel (b) but for a different input signal. The parameters used to obtain these results are provided in [36].

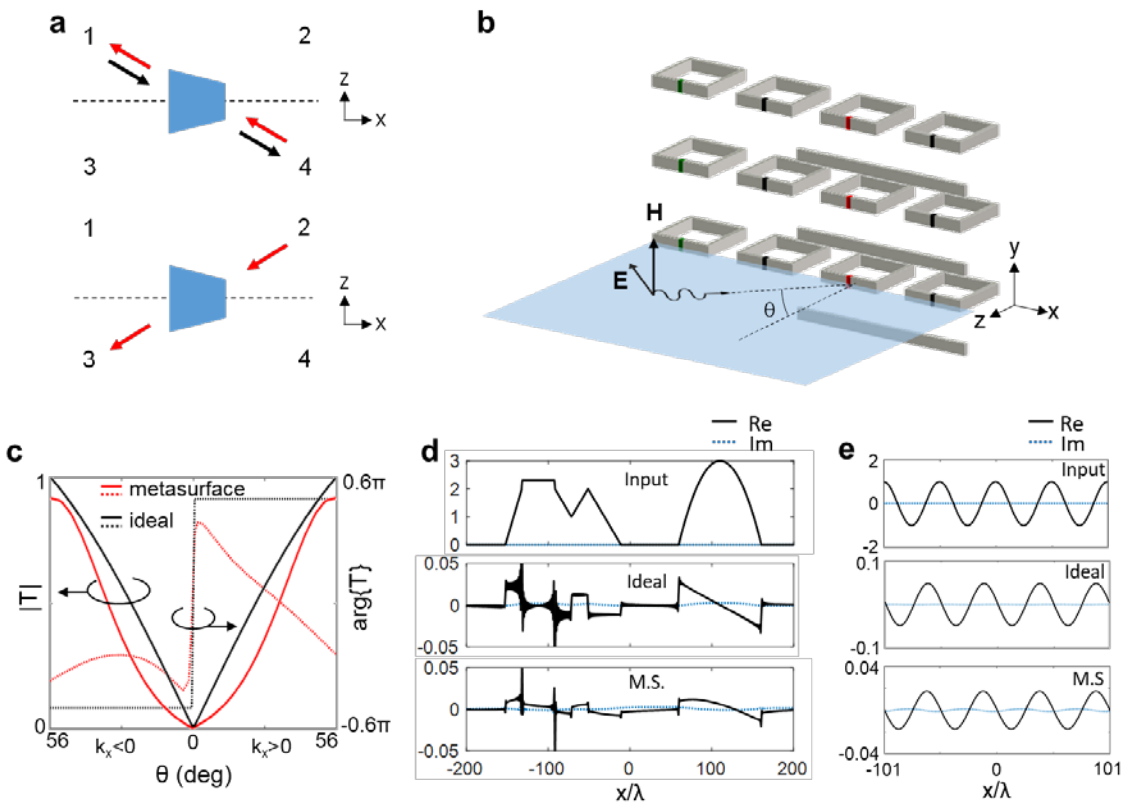

Fig.3. **First derivative operation.** (a) Limitations on the response of a metasurface with mirror symmetry with respect to the *x*-axis, imposed by reciprocity. (b) Metasurface with broken *x*- and *z*-symmetry to obtain an asymmetric response with respect to positive and negative k_x, as required in order to implement a first derivative operation. (c) Transmission versus incidence angle for the metasurface in panel (b) and for an ideal first derivative operation. The reference plane for transmission is selected at a distance that leads to a 0 deg transmission phase at normal incidence. (d) Output of an ideal first derivative operation and of the metasurface when we apply the signal at the top panel as an input. For the ideal response, we consider a cutoff angle equal to 56 deg (angle of unitary transmission for the metasurface). The input signal is discretized with a pixel size of 0.60λ. (e) Same as in panel (d) but for a different input signal. The parameters used to obtain these results are provided in [36].

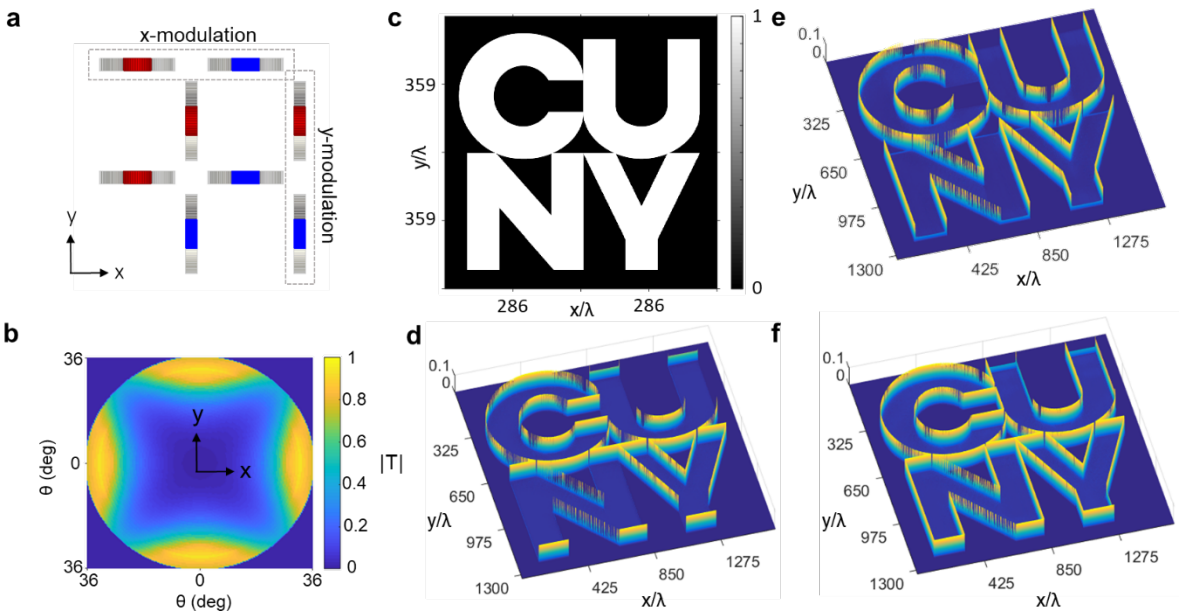

Fig. 4. Two-dimensional second derivative operation. (a) Metasurface with a 90 deg rotational symmetry to implement second derivative in 2D. (b) Transmission versus elevation and azimuthal angles θ and φ, respectively. (c) Image used to test the response of the metasurface at $f = 0.98f_0$, where f_0 is the resonance frequency of the unmodulated metasurface. For the calculation of these results, we have discretized the input signal with a pixel size of 0.86λ in each direction. (d) Output of an ideal Laplacian operation for the input image in panel (c) and illumination with an *x*-polarized wave from the normal direction. (e) Similar to panel (d) but for the metasurface in panel (a). (f) Similar to panel (e), but for illumination with unpolarized light from the normal direction. The parameters used to obtain these results are provided in [36].